PCCP

Accepted Manuscript

ROYAL SOCIETY OF CHEMISTRY

www.rsc.org/pccp

Journal Name

RSCPublishing

COMMUNICATION

Facile synthesis of SnO_2 nanocrystals anchored onto graphene nanosheets as the anode material for lithium-ion batteries

Cite this: DOI: 10.1039/x0xx00000x

Received ooth January 2012,
Accepted ooth January 2012

DOI: 10.1039/x0xx00000x

www.rsc.org/

Yanjun Zhang, Li Jiang and Chunru Wang*

SnO_2/graphene nanocomposite was prepared via a facile solvothermal process using stannous octoate as Sn source. The as-prepared SnO_2/graphene nanocomposite exhibited excellent electrochemical behavior with high reversible capacity, long cycle life and good rate capability when used as anode material for lithium ion batteries.

Introduction

As one of the most popular electrochemical energy storage devices, rechargeable lithium-ion batteries (LIBs) have been the predominant power source for modern electronic devices such as cell phones, laptop computers, and other power gadgets etc.[1,2] The electrode materials are a determining factor for the performance of LIBs. To meet the increasing demand for LIBs with high energy density, long cycle life, excellent rate capability performance, and environmental compatibility, it is highly desired to search alternative electrode materials with improved performance for next generation LIBs.[3,4] For anode materials, the commercially used graphite is insufficient to satisfy the increasing demand for batteries with high energy and power density because of its low theoretical capacity (372 mAh g^{-1}). Therefore, exploring alternative anode materials with higher reversible capacity, higher rate capability, as well as long cycle life and low cost has been a subject of extensive research nowadays. In the past decade, various advanced materials including metal oxides have been intensively studied as alternative anode materials for LIBs.[5-8] Among these metal oxides, SnO_2 has been considered to be a promising anode material for next generation LIBs because of its relatively high theoretical capacity (782 mAh g^{-1} based on 4.4 Li per molecular), natural abundance, environmental benignity, and safe lithiation potential.[9-11] However, similar to the other metal oxides electrode materials, SnO_2 anodes suffer from huge volume expansion, poor electronic conductivity and severe aggregation of Sn nanoparticles upon extended charge-discharge cycling. These shortcomings result in rapid capacity fading and poor rate capability, which hinder the practical application of the SnO_2 anodes.[12,13]

To overcome the abovementioned problems of SnO_2 anodes, various approaches have been employed. Generally, two strategies are widely explored to improve the electrochemical performance of SnO_2 as anode material for LIBs. One strategy is to design and fabricate SnO_2 with special morphologies and porous/hollow structures on the nanoscale, which would effectively sustain the huge volume expansion during lithiation and delithiation.[14-18] Another strategy is to prepare composites of SnO_2 with conductive carbonaceous materials, which would buffer the volume expansion and enhance the electronic conductivity of the SnO_2 electrodes.[19-23] Specially, building hybrid of SnO_2 nanostructures and graphene nanosheets has been regarded as one of the most effective approaches toward high performance anode materials for LIBs. The synergetic effect of SnO_2 nanostructures and graphene nanosheets is not only beneficial to improve the electronic conductivity and buffer the volume expansion during cyclic process, but also limit the growth of solid-electrolyte interphase (SEI) film and prevent the aggregation of Sn nanoparticles.[24-28]

To date, many methods have been employed to prepare SnO_2/graphene nanocomposites, such as reassembling process, mechanical mixing, atomic layer deposition (ALD) technique, gas-liquid interfacial synthesis, as well as hydrothermal methods.[29-40] From the previous reports, tin chloride ($SnCl_2$ and $SnCl_4$) were commonly used as Sn sources for the synthesis of SnO_2/graphene nanocomposites, and all the previous methods required multistep

processes (post thermal treatment) or additional chemicals (urea, hydrazine, etc.), which make the synthesis process complicated and time/energy-consuming. Therefore, it is still necessary to explore an efficient, economic, and green method for the preparation of SnO_2/graphene nanocomposites.

In this work, we report a facile one-step solvothermal method for the preparation of SnO_2/graphene nanocomposite using stannous octoate as SnO_2 sources without any additional chemicals. The as-prepared porous SnO_2/graphene nanocomposite exhibited excellent electrochemical behavior with high reversible capacity, long cycle life and high rate capability when used as anode material for LIBs.

Experimental

Fabrication of graphite oxide nanosheets: The graphite oxide (GO) nanosheets were produced from natural graphite flakes by a modified Hummers method.[41]

Synthesis of SnO_2/graphene nanocomposite: In a typical synthesis process, 0.5 mL stannous octoate and 60 mg GO nanosheets were added to 50 mL of ethanol. After being vigorously stirred for 12 h, 10 mL DI water was added to the suspension. The resulting suspension was transferred to a 100 mL Teflon autoclave, which was then heated to 160℃ in an electric oven for 10 h. Afterward, the precipitate was collected by centrifugation, washed with ethanol and deionized water for several times. After washing, the precipitate was subjected to freeze-drying, and then dried in vacuum. For comparison, bare SnO_2 nanoparticles were prepared under the same conditions but without the presence of GO.

Characterization

The X-ray diffraction (XRD) patterns of the samples were recorded on a Rigaku D/max-2500 diffractometer with CuKα radiation (λ=0.1542 nm) at 40 kV and 30 mA at a step of 0.02. Data were recorded ranging from 10° to 80°. Scanning electron microscopy (SEM) was performed on a JEOL 6701F scanning electron microscope at an accelerating voltage of 10 kV. Transmission electron microscopy (TEM) observations were carried out on FEI Tecnai F20 microscopes at 200 kV. Raman spectroscopy was recorded on a DXR Raman microscope with laser excitation wavelength of 532 nm. Thermogravimetric (TG) analysis was carried out on a TA-Q50 instrument. Nitrogen adsorption and desorption isotherms at 77 K were characterized by a Nova 2000e surface area and pore size analyzer.

Electrochemical measurements

Electrochemical measurements were performed using coin-type cells (CR2016) assembled in an argon-filled glove box. To prepare working electrodes, a mixture of the nanostructured SnO_2/graphene composites, super-P acetylene black (AC) and poly-(vinyl difluoride) (PVDF) at a weight ration of 80:10:10 in N-Methylpyrrolidone (NMP) solvent was pasted on a Cu foil (99.9%, Goodfellow). Lithium foil was used as the counter electrode. A glass fiber (GF/D) from Whatman was used as a separator. The electrolyte was 1 M $LiPF_6$ dissolved in a mixture of ethylene carbonate (EC), dimethyl carbonate (DMC) and diethyl carbonate (DEC) (1:1:1 wt%) obtained from Tianjin jinniu Power Sources Material Co., Ltd. Galvanostatic cycling of the assembled cells was carried out using an Arbin BT 2000 system in the voltage range of 0.01-3.0 V (vs. Li^+/Li) under a current density of 500 mA g^{-1}. Cyclic voltammograms (CV) were recorded at a scan rate of 0.1 mV s^{-1}. Electrochemical impedance spectral (EIS) measurements were performed on a PARSTAT 2273 advanced electrochemical system over the frequency range from 100 kHz to 10 mHz.

Results and discussion

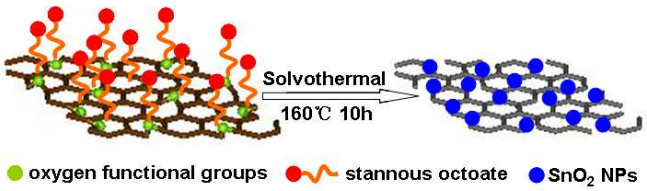

Fig. 1 Schematic illustration of the preparation process of the SnO_2/graphene nanocomposite.

SnO_2/graphene nanocomposite was successfully prepared via a facile one-step solvothermal method using stannous octoate as Sn sources without any additional chemicals. Fig. 1 represents the schematic preparation process of the SnO_2/graphene nanocomposite. When stannous octoate was mixed with GO nanosheets, the oxygen-containing functional groups on the surface of GO nanosheets acted as anchor points for the decoration of stannous octoate.[42] During the subsequent solvothermal process, GO nanosheets were reduced to graphene nanosheets, and the stannous octoate was synchronously converted to SnO_2 nanoparticles in situ anchored onto the surface of graphene nanosheets.

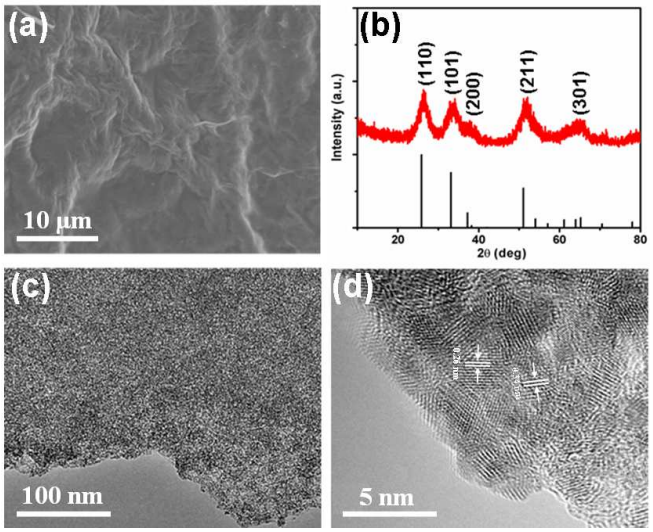

Fig. 2 (a) SEM image and (b) XRD pattern and (c) TEM image and (d) HRTEM image of the as-prepared SnO_2/graphene nanocomposite.

The morphology and structure of the as-prepared SnO_2/graphene nanocomposite were investigated by scanning electron microscopy (SEM), X-ray diffraction (XRD) and transmission electron microscopy (TEM). Fig. 2(a) depicts a typical SEM image of the as-prepared SnO_2/graphene nanocomposite. It is clear from the SEM image that the nanocomposite exhibits a curled morphology consisting of a thin wrinkled sheet-like structure. This structure suggests that the intrinsic ripples of graphene nanosheets might

develop into wavy structure in the macroscopic scale.[43,44] The size of the sheet is as large as a few micrometers. Fig. 2(b) shows the XRD pattern of the as-prepared nanocomposite. All the diffraction peaks in the XRD pattern can be indexed to the tetragonal rutile-like SnO_2 according to the standard XRD data file (JCPDS file No. 41-1445). It is obvious that all the typical diffraction peaks are broadened and are of low intensity, which proves that the size of the SnO_2 particles is very small. The TEM image shown in Fig. 2(c) reveals that uniform SnO_2 nanoparticles are homogenously distributed on the surface of the graphene nanosheets. It is noteworthy that the SnO_2 nanoparticles are tightly anchored on the surface of graphene nanosheets even after a long mechanical stirring and sonication time during the preparation of the TEM specimen, suggesting a strong interaction between SnO_2 nanoparticles and graphene nanosheets. The strong combination of SnO_2 nanoparticles and graphene nanosheets can facilitate fast electron transport through the conductive graphene matrix to SnO_2 nanoparticles, guaranteeing efficient electrochemical performance.[45] HRTEM image is displayed in Fig. 2(d). the size of the SnO_2 nanoparticles was measured to be around 3-5 nm. Void spaces can be observed between SnO_2 nanoparticles, which are beneficial for electrolyte penetration during the electrochemical test.[46] The lattice fringes with *d*-spacings of 0.26 and 0.34 nm are match well those of the (110) and (101) planes of the tetragonal SnO_2, respectively.

Raman spectroscopy was employed to identify the detailed structures of the SnO_2/graphene nanocomposite. The Raman spectra of the SnO_2/graphene nanocomposite is shown in Fig. S1. The two peaks at around 1342 and 1597 cm^{-1} can be correspond to the disordered (D) band and graphitic (G) band of carbon materials, respectively.[47] Compared with the graphene oxide nanosheets, SnO_2/graphene nanocomposite exhibits an increased D/G intensity ratio, suggesting that the oxygen-containing functional groups in graphene oxide were effectively removed and more defects were formed after solvothermal process.[48] The loading amount of SnO_2 in the nanocomposite was determined by thermogravimetric (TG) analysis (Fig. S2). Considering the fully combustion of graphene at 600℃ in air, the loading amount of SnO_2 in the nanocomposite is evaluated to be 75.9%. The Brunauer-Emmett-Teller (BET) surface area of the SnO_2/graphene nanocomposite was measured to be about 197.3 $m^2 g^{-1}$ by the N_2 sorption measurement at 77 K (Fig. S3a). The pore-size distribution (Fig. S3b) obtained from density functional theory (DFT) shows that the micropores of the SnO_2/graphene nanocomposite are mainly around 3.8 nm in diameter.

The electrochemical performance of the as-prepared SnO_2/graphene nanocomposite was first evaluated by the cyclic voltammetry. Fig. 3(a) shows the first five consecutive cyclic voltammograms (CVs) of the electrode made from the SnO_2/graphene nanocomposite in the voltage range of 0.01-3.0 V versus Li/Li^+ at a scan rate of 0.1 mV s^{-1}. There are three cathodic peaks can be observed in the first cycle. The cathodic peak located at around 0.67 V can be attributed to the formation of the solid electrolyte interphase (SEI) layer ($Li^+ + e^-$ + electrolyte → SEI), which disappeared in the following cycles.[49] The cathodic peak located at around 0.95 V can be attributed to the reduction of SnO_2 to Sn and the formation of Li_2O ($SnO_2 + 4Li^+ + 4e^- \rightarrow Sn + 2Li_2O$).[26] The clearly cathodic peak located at around 0.04 V and can be attributed to the alloying of Sn and Li ($Sn + xLi + xe^- \rightarrow Li_xSn$ ($0 \le x \le 4.4$)), and the intercalation of lithium ions into the graphene ($C_6 + 2Li^+ + 2e^- \rightarrow Li_2C_6$).[50] During the subsequent anode process, two oxidation peaks at around 0.56 and 1.25 V can be attributed to the dealloying of Li_xSn, and the partial conversion of Sn to SnO_x, respectively.[51] The difference between the first and the later cathodic scans is mainly attributed to the irreversible electrochemical reactions, corresponding to the capacity loss during the first cycle. From the second cycle onwards, the CV curves are mostly overlapped, indicating the good reversibility of the electrochemical reactions. In agreement with these CV results, correlative plateau regions can be identified in the charge-discharge voltage profiles of the SnO_2/graphene electrode, as shown in Fig. 3(b).

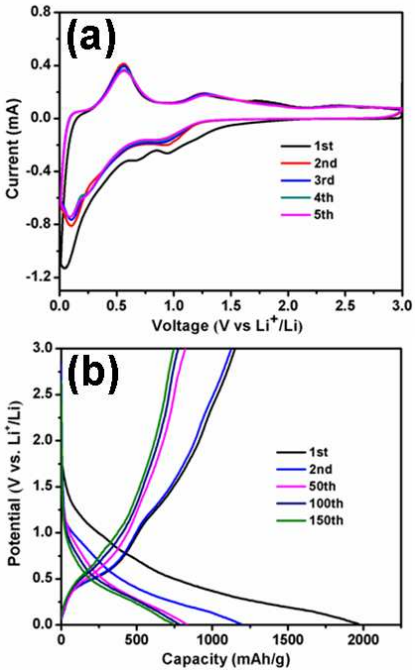

Fig. 3 (a) Cyclic voltammetry plots of the as-prepared SnO_2/graphene nanocomposite electrode at a scan rate of 0.1 mV s^{-1} in the voltage range of 0.01-3.0 V versus Li^+/Li. (b) The discharge-charge voltage profiles at a current density of 500 mA g^{-1}.

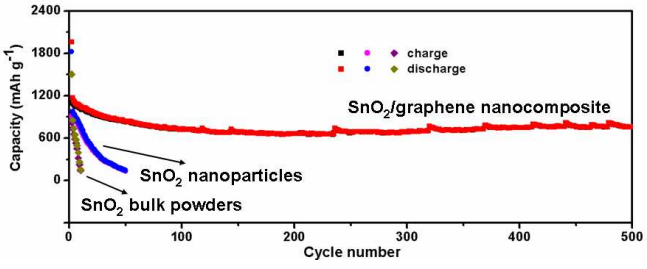

Fig. 4 Cycling performances for the electrodes of the as-prepared SnO_2/graphene nanocomposite, bare SnO_2 nanoparticles and bulk SnO_2 powders in the voltage range of 0.01-3 V (versus Li^+/Li) at a current density of 500 mA g^{-1}.

Fig. 4 displays the discharge-charge capacity versus cycle number for the SnO_2/graphene nanocomposite electrode under a current density of 0.5 A g^{-1} in the voltage range of 0.01-3.0 V versus Li^+/Li. For comparison, cycling performance of the bare SnO_2 nanoparticles and bulk SnO_2 powders were also investigated under the same

condition. As can be seen, the initial discharge and charge capacities of the SnO_2/graphene nanocomposite electrode are 1961.8 and 1119.6 mAh g^{-1}, respectively, corresponding to a Coulombic efficiency (CE) of 57.1%. The large initial capacity loss of about 42.9% can be mainly ascribed to the formation of SEI layer and the incomplete extraction of lithium from the active material.[37] The SnO_2/graphene nanocomposite electrode exhibits good capacity retention during 500 discharge-charge cycles. After 500 cycles, it still retains a capacity of 811.2 mAh g^{-1}. Note that the specific capacity values are calculated on the basis of the total mass of the SnO_2/graphene nanocomposite. In contrast, the capacities of bare SnO_2 nanoparticles and bulk SnO_2 powders (Fig. S4) fade quickly. Moreover, as shown in Fig. S5, the high CE of >95% can be achieved after initial conditioning cycles, demonstrating high reversibility of the SnO_2/graphene nanocomposite electrode.

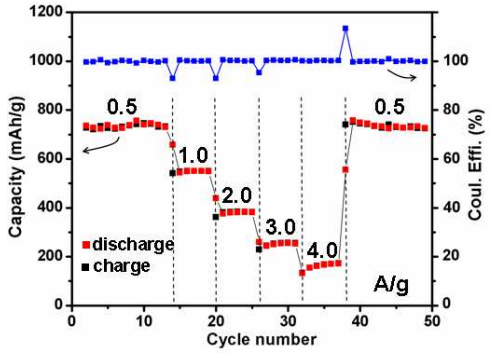

Fig. 5 Rate performances of the electrode made from the as-prepared SnO_2/graphene nanocomposite.

Excellent rate property is another indispensable capability for electrodes as advanced LIBs. Thus, the rate property of the SnO_2/graphene nanocomposite was characterized at various current densities and is shown in Fig. 5. As the current density changed from 0.5 to 4.0 A g^{-1}, specific capacities of 731.1, 551.5, 384.2, 258.3 and 170.0 mAh g^{-1} were obtained. More significantly, as the current density was reduced to low current, the capacity also recovered completely. The result indicates that the structure of SnO_2/graphene nanocomposite is stable at various current densities. The high specific capacity, long stability and outstanding rate property make the SnO_2/graphene nanocomposite a promising anode material for advanced LIBs.

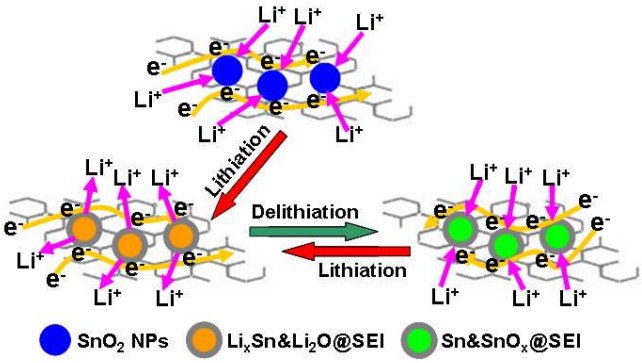

Fig. 6 Schematic illustration of the lithiation and delithiation process SnO_2/graphene nanocomposite.

The superior cycling performance and rate property may be attributed to the following several merits of the SnO_2/graphene nanocomposite, as illustrated in Fig. 6. First, the ultrasmall size of SnO_2 nanoparticles, which can significantly reduce the strain generated during the lithiation/delithiation processes and drastically shorten the diffusion path for lithium insertion/extraction as a result of the quantum size effect.[38] Second, the graphene nanosheets, which functioned as a conductive substrate to facilitate the ion/electron transport (Fig. S6) and served as a buffer to relieve the stress during cyclic process.[29] Finally, the SnO_2 nanoparticles anchored onto the graphene nanosheets can effectively enhance the strain accommodating capability and prevent the aggregation of Sn nanoparticles during the lithiation preocess.[34] These merits make as-prepared SnO_2/graphene nanocomposite a very promising anode material for LIBs.

In conclusion, SnO_2/graphene nanocomposite was successfully prepared via a facile one-step solvothermal method using stannous octoate as Sn sources without any additional chemicals. Ultrasmall SnO_2 nanoparticles were homogenously distributed on the graphene nanosheets. The as-obtained SnO_2/graphene nanocomposite was investigated as anode material for lithium ion batteries. Compared with the bare SnO_2 nanoparticles and bulk SnO_2 powders, SnO_2/graphene nanocomposite exhibited excellent electrochemical behavior with high reversible capacity, long cycle life and good rate capability. It is believed that the superior electrochemical performance of the SnO_2/graphene nanocomposite should be result from the combined merits of ultrasmall SnO_2 nanoparticles and graphene nanosheets. The high specific capacity, long stability and good rate property make the SnO_2/graphene nanocomposite a promising anode material for high performance LIBs.

Acknowledgements

This work is supported by the National Basic Research Program (No.2012CB932900), the National Basic Research Program (No. 2011CB933700), the National Key Technology Support Program (No.2012BAJ25B08) and the National Natural Science Foundation of China (No. 21121063, 11179006, 20903107).

Notes and references

Key Laboratory of Molecular Nanostructure and Nanotechnology, Beijing National Laboratory for Molecular Sciences, Institute of Chemistry, Chinese Academy of Sciences, Beijing 100190, E-mail: crwang@iccas.ac.cn.

Electronic Supplementary Information (ESI) available: Additional Raman spectra, TGA curve, N_2 adsorption-desorption isotherms and SEM images. See DOI: 10.1039/c000000x/

1 Y. Idota, T. Kubota, A. Matsufuji, Y. Maekawa, T. Miyasaka, *Science*, 1997, **276**, 1395.
2 J. M. Tarascon, M. Armand, *Nature*, 2001, **414**, 359.
3 Y. G. Guo, J. S. Hu, L. J. Wan, *Adv. Mater.*, 2008, **20**, 2878.
4 P. G. Bruce, B. Scrosati, J. M. Tarascon, *Angew. Chem. Int. Ed.*, 2008, **47**, 2930.
5 M. V. Reddy, G. V. Subba Rao, B. V. R. Chowdari, *Chem. Rev.*, 2013, **113**, 5364.
6 M. N. Obrovac, V. L. Chevrier, *Chem. Rev.*, 2014, **114**, 11444.
7 X. D. Xu, W. Liu, Y. Kim, J. Cho, *Nano Today*, 2014, **9**, 604.
8 H. Kim, G. Jeong, Y. U. Kim, J. H. Kim, C. M. Park, H. J. Sohn, *Chem. Soc. Rev.*, 2013, **42**, 9011.
9 G. Derrien, J. Hassoun, S. Panero, B. Scrosati, *Adv. Mater.*, 2007, **19**, 2336.

10 X. W. Lou, C. M. Li, L. A. Archer, *Adv. Mater*., 2009, **21**, 2536.
11 C. Wang, Y. Zhou, M. Ge. X. Xu, Z. Zhang, J. Jiang, *J. Am. Chem. Soc*., 2010, **132**, 46.
12 I. A. Courtney, J. R. Dahn, *J. Electrochem. Soc*., 1997, **144**, 2943.
13 M. Winter, J. O. Besenhard, M. E. Spahr, P. Novak, *Adv. Mater*., 1998, **10**, 725.
14 T. Yang, B. Lu, *Phys. Chem. Chem. Phys*., 2014, **16**, 4115.
15 Z. Y. Wang, D. Y. Luan, F. Y. C. Boey, X. W. Lou, *J. Am. Chem. Soc*., 2011, **133**, 4738.
16 J. Z. Wang, N. Du, H. Zhang, J. X. Yu, D. R. Yang, *J. Phys. Chem. C*, 2011, **115**, 11302.
17 R. Liu, S. C. Yang, F. Wang, X. G. Lu, Z. M. Yang, B. J. Ding, *ACS Appl. Mater. Interfaces*, 2012, **4**, 1537.
18 Y. J. Hong, M. Y. Son, Y. C. Kang, *Adv. Mater.*, 2013, **25**, 2279.
19 N. R. Srinivasan, S. Mitra, R. Bandyopadhyaya, *Phys. Chem. Chem. Phys.*, 2014, **16**, 6630.
20 H. Liu, S. Chen, G. X. Wang, S. Z. Qiao, *Chem. Eur. J.*, 2013, **19**, 16897.
21 M. He, L. X. Yuan, X. L. Hu, W. X. Zhang, J. Shu, Y. H. Huang, *Nanoscale*, 2013, **5**, 3298.
22 J. Liang, X. Y. Yu, H. Zhou, H. B. Wu, S. J. Ding, X. W. Lou, *Angew. Chem. Int. Ed.*, 2014, **53**, 12803.
23 L. Zhang, K. N. Zhao, W. W. Xu, Y. F. Dong, R. Xia, F. N. Liu, L. He, Q. L. Wei, M. Y. Yan, L. Q. Mai, *Phys. Chem. Chem. Phys.*, 2015, **17**, 7619.
24 S. M. Paek, E. J. Yoo, I. Honma, *Nano Lett.*, 2009, **9**, 72.
25 J. F. Liang, Y. Zhao, L. Guo, L. D. Li, *ACS Appl. Mater. Interfaces*, 2012, **4**, 5742.
26 X. S. Zhou, L. J. Wan, Y. G. Guo, *Adv. Mater*., 2013, **25**, 2152.
27 C. H. Xu, J. Sun, L. Gao, *J. Mater. Chem*., 2012, **22**, 975.
28 Y. F. Dong, Z. B. Zhao, Z. Y. Wang, Y. Liu, X. Z. Wang, J. S. Qiu, *ACS Appl. Mater. Interfaces*, 2015, **7**, 2444.
29 S. J. R. Prabakar, Y. H. Hwang, E. G. Bae, S. Shim, D. Kim, M. S. Lah, K. S. Sohn, M. Pyo, *Adv. Mater.*, 2013, **25**, 3307.
30 L. S. Zhang, L. Y. Jiang, H. J. Yan, W. Wang, W. G. Song, Y. G. Guo, L. J. Wan, *J. Mater. Chem.*, 2010, **20**, 5462.
31 F. Ye, B. Zhao, R. Ran, Z. Shao, *Chem. Eur. J*., 2014, **20**, 4055.
32 X. Li, X. Meng, J. Liu, D. Geng, Y. Zhang, M. Banis, Y. Li, R. Li, X. Sun, M. Cai, *Adv. Funct. Mater*., 2012, **22**, 1647.
33 P. C. Lian, X. F. Zhu, S. Z. Liang, Z. Li, W. S. Yang, H. H. Wang, *Electrochimica Acta*, 2011, **56**, 4532.
34 J. F. Liang, W. Wei, D. Zhong, Q. L. Yang, L. D. Li, L. Guo, *ACS Appl. Mater. Interfaces*, 2012, **4**, 454.
35 S. K. Park, S. H. Yu, N. Pinna, S. Woo, B. Jang, Y. H. Chung, Y. H. Cho, Y. E. Sung, Y. Z. Piao, *J. Mater. Chem.*, 2012, **22**, 2520.
36 X. W. Liu, J. X. Cheng, W. H. Li, X. W. Zhong, Z. Z. Yang, L. Gu, Y. Yu, *Nanoscale*, 2014, **6**, 7817.
37 C. Zhong, J. Z. Wang, Z. X. Chen, H. K. Liu, *J. Phys. Chem. C*, 2011, **115**, 25115.
38 R. Ravikumar, S. Gopukumar, *Phys. Chem. Chem. Phys*., 2013, **15**, 3712.
39 S. J. Ding, D. Y. Luan, F. Y. C. Boey, J. S. Chen, X. W. Lou, *Chem. Commun*., 2011, **47**, 7155.
40 S. Yang, W. B. Yue, J. Zhu, Y. Ren, X. J. Yang, *Adv. Funct. Mater*., 2013, **23**, 3570.
41 W. S. Hummers, R. E. Offeman, *J. Am. Chem. Soc*., 1958, **80**, 1339.
42 Y. Chen, B. H. Song, R. M. Chen, L. Lu, J. M. Xue, *J. Mater. Chem. A*, 2014, **2**, 5688.
43 A. Fasolino, J. H. Los, M. I. Katsnelson, *Nat. Mater.*, 2007, **6**, 858.
44 J. C. Meyer, A. K. Geim, M. I. Katsnelson, K. S. Novoselov, T. J. Booth, S. Roth, *Nature*, 2007, **446**, 60.
45 X. Wang, X. Q. Cao, L. Bourgeois, H. Guan, S. M. Chen, Y. T. Zhong, D. M. Tang, H. Q. Li, T. Y. Zhai, L. Li, Y. Bando, D. Golberg, *Adv. Funct. Mater.*, 2012, **22**, 2682.
46 D. N. Wang, X. F. Li, J. J. Wang, J. L. Yang, D. S. Geng, R. Y. Li, M. Cai, T. K. Sham, X. L. Sun, *J. Phys. Chem. C*, 2012, **116**, 22149.
47 A. C. Ferrari, J. Robertson, *Phy. Rev. B*, 2000, **61**, 14095.
48 A. Gupta, G. Chen, P. Joshi, S. Tadigadapa, P. C. Eklund, *Nano Lett*., 2006, **6**, 2667.
49 J. Lin, Z. W. Peng, C. S. Xiang, G. D. Ruan, Z. Yan, D. Natelson, J. M. Tour, *ACS Nano*, 2013, **7**, 6001.
50 J. Yao, X. P. Shen, B. Wang, H. K. Liu, G. X. Wang, *Electrochem. Commun.*, 2009, **11**, 1849.
51 H. Li, X. J. Huang, L. Q. Chen, *J. Power Sources*, 1999, **81**, 340.